Ecological Modelling 265 (2013) 124–135

Contents lists available at SciVerse ScienceDirect

Ecological Modelling

journal homepage: www.elsevier.com/locate/ecolmodel

Simulation of canopy CO_2/H_2O fluxes for a rubber (*Hevea brasiliensis*) plantation in central Cambodia: The effect of the regular spacing of planted trees

Tomo'omi Kumagai[a,*], Ryan G. Mudd[b], Yoshiyuki Miyazawa[c], Wen Liu[b], Thomas W. Giambelluca[b], Nakako Kobayashi[a], Tiva Khan Lim[d], Mayuko Jomura[e], Kazuho Matsumoto[f], Maoyi Huang[g], Qi Chen[b], Alan Ziegler[h], Song Yin[d]

[a] *Hydrospheric Atmospheric Research Center, Nagoya University, Chikusa-ku, Nagoya 464-8601, Japan*
[b] *Department of Geography, University of Hawai'i at Mānoa, Honolulu, HI 96822, USA*
[c] *Research Institute for East Asia Environments, Kyushu University, Motooka, Fukuoka 811-0395, Japan*
[d] *Cambodian Rubber Research Institute, Phnom Penh, Cambodia*
[e] *College of Bioresource Sciences, Nihon University, Fujisawa, Kanagawa 252-0880, Japan*
[f] *Faculty of Agriculture, University of the Ryukyus, Chihara, Okinawa 903-0213, Japan*
[g] *Atmospheric Sciences and Global Change Division, Pacific Northwest National Laboratory, Richland, WA 99352, USA*
[h] *Department of Geography, National University of Singapore, 21 Lower Kent Ridge Road, 117570, Singapore*

ARTICLE INFO

Article history:
Received 18 February 2013
Received in revised form 13 June 2013
Accepted 13 June 2013

Keywords:
Eddy covariance
Soil–plant–atmosphere continuum
Canopy photosynthesis
Canopy transpiration
Clumping factor
Canopy gap

ABSTRACT

We developed a soil-vegetation-atmosphere transfer (SVAT) model applicable to simulating CO_2 and H_2O fluxes from the canopies of rubber plantations, which are characterized by distinct canopy clumping produced by regular spacing of plantation trees. Rubber (*Hevea brasiliensis* Müll. Arg.) plantations, which are rapidly expanding into both climatically optimal and sub-optimal environments throughout mainland Southeast Asia, potentially change the partitioning of water, energy, and carbon at multiple scales, compared with traditional land covers that are being replaced. Describing the biosphere–atmosphere exchange in rubber plantations via SVAT modeling is, therefore, important to understanding the impacts on environmental processes. The regular spacing of plantation trees creates a peculiar canopy structure that is not well represented in most SVAT models, which generally assume a non-uniform spacing of vegetation. Herein we develop a SVAT model applicable to a rubber plantation and an evaluation method for its canopy structure, and examine how the peculiar canopy structure of rubber plantations affects canopy CO_2 and H_2O exchanges. Model results are compared with measurements collected at a field site in central Cambodia. Our findings suggest that it is crucial to account for intensive canopy clumping in order to reproduce observed rubber plantation fluxes. These results suggest a potentially optimal spacing of rubber trees to produce high primary productivity and water use efficiency.

1. Introduction

Rubber (*Hevea brasiliensis* Müll. Arg.) is among the major tropical economic tree crops of the world, including Southeast Asia, which is outside the native range of rubber. Originating in the Amazonian tropical rainforests, rubber is intrinsically suitable for climates that are warm and moist throughout the year (Priyadarshan, 2003; Priyadarshan et al., 2005). However, selective breeding of *Hevea* clones has facilitated the expansion of rubber plantations into relatively cool and dry environments, such as those found in montane and monsoonal regions of mainland Southeast Asia. Rubber is now cultivated profitably in many "non-traditional" areas previously determined as unsuitable (Qiu, 2009).

The Association of Natural Rubber Producing Countries (ANRPC) (2010) estimated that from 2003 to 2010 more than 1,500,000 ha of land were converted to rubber in southern China, Thailand, Vietnam, and Cambodia. Rubber is currently expanding rapidly in non-traditional areas of Myanmar, Laos, and India. In the uplands of mainland Southeast Asia, about 9% of the current vegetation, such as evergreen broadleaf trees and swidden-related secondary vegetation, is projected to be replaced by tree plantations and other diversified farming systems by 2050 (Fox et al., 2012). Almost half

* Corresponding author at: Hydrospheric Atmospheric Research Center, Nagoya University, Furo-cho, Chikusa-ku, Nagoya, Aichi 464-8601, Japan.
Tel.: +81 52 789 3478; fax: +81 52 788 6206.
E-mail address: tomoomikumagai@gmail.com (T. Kumagai).

0304-3800/$ – see front matter © 2013 Elsevier B.V. All rights reserved.
http://dx.doi.org/10.1016/j.ecolmodel.2013.06.016

of this transition is expected to be due to the expansion of rubber plantation, which is the most rapidly expanding tree crop in the region (Fox et al., 2012).

Numerous potential negative ecological and environmental consequences of converting primary and secondary forests into rubber plantations have been suggested: decrease in biodiversity, reduction of total carbon biomass, alteration of the hydrological regime, and acceleration of erosion (Wu et al., 2001; Mann, 2009; Qiu, 2009; Ziegler et al., 2009a,b, 2012; Guardiola-Claramonte et al., 2010; Tan et al., 2011). On the other hand, a considerable proportion of rubber plantations have been converted from intensive annual cropping systems such as cassava, sugar cane, soybean, maize, and rice, thus land use history is an important factor when assessing the environmental impacts of conversion to rubber. Increasingly, the loss of community-based resources such as non-timber forest products and agricultural land must be weighed against the economic benefits, as rubber cultivation provides for the livelihoods of smallholders and their workers, together numbering in the millions (Simien and Penot, 2011). Moreover, some studies reported that carbon sequestration in the case of rubber plantations cultivation replacing non-forested areas could act as a carbon sink (Wauters et al., 2008), and that water use of rubber plantations was not as high as anticipated (Isarangkool Na Ayutthaya et al., 2011; Carr, 2012). Of concern to our research, large-scale land use changes to rubber plantations may have important implications for local-to-regional carbon and water balances, but they still remain unclear. Hindering the ability to predict and understand these changes are limitations to existing soil-vegetation-atmosphere transfer (SVAT) models and insufficient data for model evaluation, the subject of this investigation.

Our experience shows that SVAT models, parameterized by independently collected leaf-level ecophysiological measurements and not calibrated or parameterized by canopy-level flux measurements, can be applied for examining the effects of ecophysiological functions on the formation of the ecosystem fluxes over natural tropical forests (e.g., Tanaka et al., 2003, 2004; Kumagai et al., 2006; Kumagai and Kume, 2012). In general, tree plantations are planted in rows for management purposes, which may cause highly clumped foliage and canopy gaps between rows, particularly for young stands before canopy closure. Thus, rubber and other tree plantations represent a modeling challenge, because the regular tree spacing violates a basic model assumption of random clumping as it affects within-canopy radiative transfer (cf. Chen and Cihlar, 1995).

In this study we develop both a SVAT model that is applicable for rubber plantations and a method to evaluate their canopy structure. We then examine how the peculiar canopy structure affects the canopy CO_2 and H_2O exchanges by comparing model results with eddy flux measurements collected at a field site in Cambodia. Firstly, the SVAT model was validated using data from a 10-day period of eddy flux data selected from a dataset representing two years of field observations. After the validation, we assessed the effects of the rubber canopy structure on the ecosystem flux processes, as an application of the SVAT model. This is intended as a first step in the investigation of the impact of land use change, especially the rapid expansion of tree plantations, on water and carbon cycling in this region.

2. Model description

The SVAT model (see Kumagai et al., 2006) used in this study consists of three major submodels: (1) a model for energy, water and radiation conservation; (2) an ecophysiological model for stomatal opening and carbon assimilation; and (3) a model for turbulent diffusion. The total computation domain comprising a canopy and atmosphere above it are divided into 50 and 150 layers, respectively. All equations in this model are solved at each layer. In the present model we added a treatment of canopy water balance, including interception, throughfall, and water storage on the leaves. We also accounted for the highly clumped foliage characteristic of rubber plantations. A brief description of this modeling scheme, together with explanations regarding new components, is provided below (cf. Kumagai et al., 2006).

2.1. Radiative transfer and energy and water balance at both leaf and soil surface level

When considering the leaf-scale energy balance together with photosynthesis within a forest canopy, the radiative transfer through the canopy must be determined. Direct beam and diffuse irradiance must be considered separately due to their different attenuations in the canopy. The probability of no contact within a canopy layer for beam irradiance (P_b) needs to be formulated for describing the direct irradiance transfer within the canopy. This formulation includes the leaf area density (a_{leaf}), the beam extinction function of solar elevation and leaf angle distribution within a given layer (see Goudriaan, 1977).

In rubber plantations, rubber trees are planted with a regular spacing, and thus, their foliage and crowns are highly clumped. In the model used in this study we incorporate a clumping factor (Ω) in the P_b equation by replacing a_{leaf} with Ωa_{leaf} (see Chen et al., 2008). Details on theory of Ω and practical method to obtain the Ω in the study field will be described later. The probability of no contact within a canopy layer for diffuse irradiance (P_d) is calculated by integrating P_b over the solid angles of the sky hemisphere. Downward and upward long-wave radiation (R_L) transfer within a canopy follows theories of diffuse irradiance transfer. However, it must be noted that R_L is emitted from any plant body within the canopy.

Both direct and diffuse solar radiation can be further divided into photosynthetic active radiation (PAR) and near-infrared radiation (NIR) according to their different absorption by leaves. Fortunately, approximately half the global solar radiation (R_s) over the canopy is in the form of PAR while the other half is in the form of NIR (Campbell and Norman, 1998), enabling estimates of R_s penetration inside the canopy. The absorbed PAR or NIR within a canopy layer between z (the height from the ground) and $z+\Delta z$, ΔS, is defined as:

$$\Delta S_b = (1-\eta-\xi)(1-P_b)S_{b\_z+\Delta z} \quad (1)$$

$$\Delta S_d^{\downarrow} = (1-\eta-\xi)(1-P_d)S_{d\_z+\Delta z}^{\downarrow} \quad (2)$$

$$\Delta S_d^{\uparrow} = (1-\eta-\xi)(1-P_d)S_{d\_z}^{\uparrow} \quad (3)$$

where η and ξ are the leaf transmissivity and reflectivity, respectively, for PAR or NIR, and S is PAR or NIR at the given height. The subscripts b and d denote direct beam and diffuse irradiation, respectively, and superscript arrows denote the direction of the irradiation. Because P_b and P_d are complex functions of the leaf area density, leaf angle distribution and foliage clumping factor within a given canopy layer and for a given solar geometric direction (see Kumagai et al., 2006), Eqs. (1) through (3) are not readily solved. The total absorbed solar radiation within the canopy layer is then calculated as the sum of the absorbed PAR and NIR, both of which are calculated by Eqs. (1) through (3). Sunlit leaves receive the beam and the upward and downward diffuse radiation, while shaded leaves only receive upward and downward diffuse radiation. Therefore, the irradiance absorption and energy balance need to be computed separately for sunlit and shaded leaves (see Kumagai et al., 2006).

The energy balance at the soil surface for computing T_{soil}, is expressed by:

$$R_{sab\_soil} + R_{L\_down}(0) - \varepsilon_s \sigma (T_{soil} + 273)^4 = G_{soil} + LE_{soil} + H_{soil} \quad (4)$$

where R_{sab_soil} is the total R_s absorbed by the soil surface, $R_{L\_down}(0)$ is downward R_L at $z = 0$, ε_s is the soil emissivity, σ is the Stefan–Boltzmann constant (5.67×10^{-8} W m^{-2} K^{-4}), and LE_{soil} and H_{soil} are latent and sensible heat fluxes at the soil surface, respectively. LE_{soil} and H_{soil} are the functions of T_{soil}, as described by the products of the transport conductance and the concentration difference. In addition, the soil surface moisture availability was also used for the LE_{soil} computation (see Kumagai et al., 2006). G_{soil} is soil heat storage, assumed to be G_1 R_{sab_soil} $\sin[2\pi(t - G_2)/24] + G_3$, where t is the hour of the day and G_1, G_2 and G_3 are fitting parameters.

The water storage on the leaf surface is given as (see Watanabe and Mizutani, 1996):

$$\frac{dW_{leaf}}{dt} = F_{th}(1 - P_b) - F_{out\_leaf} \quad (5)$$

where W_{leaf} the amount of stored water per leaf area index within a canopy layer (i.e., $a_{leaf}\, dz$), t is time, F_{th} is throughfall within the canopy layer and rainfall above the canopy, and F_{out_leaf} is the wet leaf evaporation (positive) or condensation (negative) rates. Note that the P_b here is the same one for the radiative transfer, but a variable for rainfall drops direction was used instead of the solar geometric direction in the equation. To take into consideration the case $W_{leaf} > W_{leaf\_max}$ (water storage capacity per leaf area index within a canopy layer), when overflow from a leaf occurs, F_{th} is formulated as:

$$F_{th}(z) = \max(0, W_{leaf} - W_{leaf\_max}) a_{leaf} dz + P_b F_{th}(z + \Delta z) \quad (6)$$

Note that the latent heat flux term in the equation of the energy balance on the leaf surfaces considers water vapor fluxes as evaporation from the wet leaf surface, transpiration from the dry leaf surface (described next), and condensation to both the wet and dry surfaces.

2.2. Leaf-level physiological functions

The leaf-level scalar source strengths, i.e., leaf sensible heat (H_{leaf}: W m^{-2}), evapotranspiration (E_{leaf}: kg m^{-2} s^{-1}) and photosynthesis rate (A_{leaf}: μmol m^{-2} s^{-1}) are derived from physiological controls using:

$$H_{leaf} = 2 m_a c_p g_{ah} (T_{leaf} - T) \quad (7)$$

$$E_{leaf} = m_e g_{aw} \left[\frac{g_{sw}}{g_{aw} + g_{sw}} \left(1 - \frac{W_{leaf}}{W_{leaf\_max}} \right) + \frac{W_{leaf}}{W_{leaf\_max}} \right] \frac{[e_{sat}(T_{leaf}) - e]}{p_a} \quad (8)$$

$$A_{leaf} = \left(1 - \frac{W_{leaf}}{W_{leaf\_max}} \right) g_{ac} (C_a - C_s) \quad (9)$$

$$= \left(1 - \frac{W_{leaf}}{W_{leaf\_max}} \right) g_{sc} (C_s - C_i) \quad (10)$$

where m_a and m_e are the molecular weights of air and water (kg mol^{-1}), respectively, T is air temperature (K), $e_{sat}(T_{leaf})$ and e are the saturation vapor pressure at leaf temperature (T_{leaf}) and atmospheric water vapor pressure (Pa), respectively, p_a is the atmospheric pressure (Pa), and C_s, C_a and C_i are the CO_2 concentrations (μmol mol^{-1}) of air inside and outside the laminar boundary layer of leaves and within the stomatal cavity, respectively. g_{ah}, g_{aw} and g_{ac} are the boundary layer conductances for heat, water vapor and CO_2 (mol m^{-2} s^{-1}), respectively, calculated according to Campbell and Norman (1998).

g_{sw} and g_{sc} are the stomatal conductances for water vapor and CO_2 (mol m^{-2} s^{-1}), respectively. g_{sc} is linked to A_{leaf}, the relative humidity of air inside the boundary layer of a leaf (h_s) and C_s, as described by Ball et al. (1987) and Collatz et al. (1991), and is given by:

$$g_{sc} = m_L \frac{A_{leaf} h_s}{C_s} + b_L \quad (11)$$

where m_L and b_L are the slope and intercept, respectively, and were obtained by linear regression analysis of data from leaf-level gas exchange measurements. g_{sw} is obtained from $g_{sw} = 1.6\, g_{sc}$, where 1.6 is the ratio of diffusivities of water and CO_2 in air (von Caemmerer and Farquhar, 1981).

A_{leaf} was computed using the biochemical model of Farquhar et al. (1980) and Collatz et al. (1991) as a minimum value of the gross rate of photosynthesis limited by the rate of RuBP regeneration through electron transport (J_E), RuBP carboxylase-oxygenase (Rubisco) activity (J_C) and the export rate of synthesized sucrose (J_S), as:

$$A_{leaf} = \min \{ J_E, J_C, J_S \} - R_d \quad (12)$$

where R_d is the respiration rate during the day but in the absence of photorespiration. The formulation and parameterization of J_E, J_C, J_S and R_d as a function of PAR absorbed by the leaf, CO_2 concentration within the stomatal cavity and leaf temperature is used from Farquhar et al. (1980), Farquhar and Wong (1984), Collatz et al. (1991) and de Pury and Farquhar (1997). The photosynthesis model constants can be determined according to Badger and Collatz (1977), Farquhar et al. (1980), von Caemmerer et al. (1994) and de Pury and Farquhar (1997). The maximum carboxylation rate when RuBP is saturated (V_{cmax}: μmol m^{-2} s^{-1}) and the potential rate of whole-chain electron transport (J_{max}: μmol m^{-2} s^{-1}) used in these calculations are expressed as non-linear functions of temperature using values at 25 °C (V_{cmax_25} and J_{max_25}, respectively); the formulations of which are given in de Pury and Farquhar (1997). In addition, R_d is expressed as a non-linear function of temperature using R_d at 25 °C (R_{d_25}), which was assumed to be linearly related to V_{cmax_25} (as in Collatz et al., 1991). Practically, both J_{max_25} and R_{d_25} are related to V_{cmax_25}, and hence, V_{cmax_25} is the key parameter in the leaf photosynthesis model.

2.3. Momentum and scalar transport

The momentum and scalar continuity and turbulent flux equations are obtained by assuming a steady state planar-homogeneous and that the turbulent Schmidt number for scalar is unity, and by applying a first-order turbulent closure scheme with time and horizontal averaging:

$$0 = \frac{\partial}{\partial z} \left(K_t \frac{\partial \varphi}{\partial z} \right) + S_\phi \quad (13)$$

where K_t is the eddy turbulent diffusivity (m^2 s^{-1}), and φ is a variable such as wind speed (U: m s^{-1}), T, specific humidity (q: kg kg^{-1}), and CO_2 concentration in the air (c: μmol m^{-3}). S_φ is a source (or sink) terms for φ, due to drag force and mass release (or uptake) by the ensemble of leaves within the averaging plane, given by:

$$S_U = C_d a_{leaf} U^2 \quad (14)$$

$$S_T = \frac{1}{\rho_a c_p} (H_{leaf\_sl} a_{leaf\_sl} + H_{leaf\_sh} a_{leaf\_sh}) \quad (15)$$

$$S_q = \frac{1}{\rho_a} (E_{leaf\_sl} a_{leaf\_sl} + E_{leaf\_sh} a_{leaf\_sh}) \quad (16)$$

$$S_c = -(A_{leaf\_sl}a_{leaf\_sl} + A_{leaf\_sh}a_{leaf\_sh}) \quad (17)$$

where C_d is the drag coefficient (0.3), ρ_a is the density of air ($kg\,m^{-3}$), and c_p is the specific heat of air at constant pressure ($J\,kg^{-1}\,K^{-1}$). Subscripts sl and sh denote sunlit and shaded leaves, respectively. In general, first-order closure principles are applicable when the production term is balanced by the dissipation term in the scalar flux budget with minimal contributions from the gradients in the turbulent flux transport terms, and this condition is generally satisfied in the studied rubber canopy (see Manzoni et al., 2011).

3. Materials and methods

3.1. Site description

The experiments were carried out at a 6.25-ha plot in an experimental rubber plantation within the 994-ha Cambodian Rubber Research Institute (CRRI) in Kampong Cham Province, Cambodia (11°57′ N, 105°34′ E, ca. 50 m a.s.l.). The experimental rubber plantation is on a level plain in basaltic latosols. The soil texture is clay with 8.4% fine sand, 10.1% coarse silt, 19.5% fine silt and 55.1% clay. The climate is governed by the Asian Monsoon, showing two distinct seasons: a wet season (approximately May–October) and a dry season (approximately November–April). The annual precipitation in 2010 and 2011 were 1332 and 1545 mm, respectively. Rainy seasons extended from late-May to late-November in 2010; late-April to mid-November in 2011. The annual mean temperature was significantly higher in 2010 (28.0 °C) than in 2011 (27.0 °C). For both years, maximum monthly averages occurred in April–May; minimums occurred in December–January.

In the study plot, all rubber trees are of clone RRIC 100 and bred under rainfed conditions. All the trees were planted in 2004 (i.e., 7 years old in 2011) with regular spacing at 6-m in north–south direction and 3-m in east–west direction, resulting in a potential tree density of 555 trees ha^{-1} (see Fig. 1). Due to tree mortality, approximately 20% of trees in mature stands are missing, thus the estimated tree density of the study plot is 458 trees ha^{-1}. Stem diameters were measured at 1.7 m height above the ground so as not to overlap the tapping panel which starts at 1.3 m. Latex tapping was initiated in November, 2010, and continued through the study period. Mean stem diameter was 13.3 cm (standard deviation (SD) = 2.3 cm, n = 99) in February 2010. This increased to 15.3 cm (SD = 2.3 cm) in March 2012. Mean canopy height was 11.4 m in January 2010, 12.9 m in March 2011, and 14.3 m in March 2012. Various species of herbaceous plants and shrubs occupy the understory; and their density is moderately high.

3.2. Meteorological and flux measurements

A 30-m-tall canopy tower was constructed at the study plot for micrometeorological and eddy flux measurements. A four-component radiation sensor (NR01, Hukseflux, Delft, Netherlands) and an air temperature and humidity sensor (HMP45C, Campbell Scientific, Logan, UT) were installed about approximately 30 m above the forest floor. Precipitation was recorded by two tipping bucket rain gauges (TE-525, Texas Electronics, Inc., Dallas, TX) mounted at a height of 15 m (close the canopy top to reduce wind-related measurement error) on opposite sides of the tower. To minimize bias from tower interference, rainfall from the upwind gauge was used, based on mean wind direction observed in each 30-min interval. Both rain gauges were dynamically calibrated, with regression equations relating mm/tip to the 30-min rainfall rate, developed by simulating an appropriate range of rainfall intensities for each rain gauge after mounting on the tower. Samples were taken at 10 Hz for radiation and air temperature, humidity and pressure and

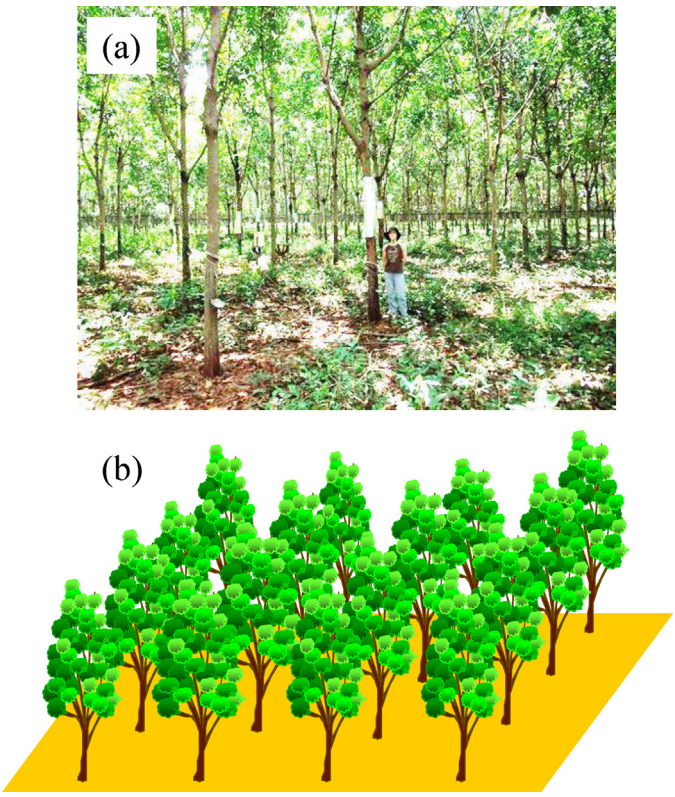

Fig. 1. (a) Photograph of the studied plot in Cambodian Rubber Research Institute (CRRI) experimental plantation, and (b) schematic representation of the rubber tree stand.

averaged over 30 min, and precipitation was measured by counting tipping bucket tips (CR3000 and CR23X, Campbell Scientific). We also sampled mean air temperature and humidity at heights of 0.5, 1.5, 4, 8, 15, and 25 m using a series of ventilated sensors with a data logger (HOBO Weather Station Data Logger and Temperature RH Smart Sensor, Onset, Pocasset, MA). Volumetric soil moisture content was measured at 5, 10, 20, 30, and 50 cm below the forest floor every 30 s using amplitude-domain reflectometry (ADR) sensors (ThetaProbe ML2x, Delta-T Devices, Cambridge, UK) and averaged over 30 min (CR1000, Campbell Scientific).

The latent heat flux (LE), sensible heat flux, and CO_2 flux were measured via the eddy covariance technique. A three-dimensional sonic anemometer (CSAT3, Campbell Scientific) and an open-path CO_2/H_2O analyzer (LI-7500, Li-Cor, Lincoln, NE) were installed at a height of 30.1 m above the ground. Wind speeds and gas concentration time series were all sampled and stored at 10 Hz. All variances and covariances required for the eddy covariance flux estimates were computed over a 30-min averaging interval. The details of screening, filtering, and post-processing of 10 Hz data to compute 30-min fluxes are identical to those described in Giambelluca et al. (2009). The flux observation footprint was analyzed for the period of this study using the method of Kormann and Meixner (2001). Results indicated that 78% of observed fluxes originated within the rubber plantation (boundary at a minimum distance of 600 m from the tower and at least 1000 m in most directions), with an average distance to the point of maximum contribution of 18.5 m, well within the study plot.

CO_2 concentration profile measurements within and above the canopy were carried out at 0.5, 1.5, 4, 8, 15, and 25 m above ground level using tower. Air samples were obtained by an auto solenoid switching system with diaphragm pumps; and CO_2 concentrations were measured using a closed-path CO_2 infrared gas analyzer (LI-820, Li-Cor). The net ecosystem CO_2 exchange (NEE) was derived

as the sum of the above-canopy CO_2 flux, which was obtained using the eddy covariance system above the canopy, and within-canopy storage flux, which was determined by quantifying the rate of change of the CO_2 concentration in the air column within the canopy.

3.3. Leaf-level physiology and soil respiration measurements

Leaf gas exchange measurements from the top of the canopy to 2.6 m below the top of the canopy were conducted during the period 27 November–2 December 2011 using a portable IRGA (LI-6400, Li-Cor). The main leaf physiological parameters, i.e., m_L and b_L in Eq. (11) and V_{cmax_25} in Eq. (12), were computed as their vertical profiles from the $g_{sc} - A_{leaf}\, h_s/C_s$ and the $A_{leaf} - C_i$ relationships, respectively, which were derived from the in situ gas exchange measurements. We assumed $J_{max} = 2\,V_{cmax}$ and $R_d = 0.02\,V_{cmax}$ (see Eq. (12)) with considering Wullschleger (1993) and this study's observation. Note that we conducted leaf gas exchange measurements in September and October, 2010, May, November and December, 2011, January, March, May, August, 2012, and February, 2013, and based on these observations we confirmed that m_L and V_{cmax_25} of rubber trees at the study site remained relatively constant throughout the year except just before leaf abscission when m_L and V_{cmax_25} dropped. Thus, we used the leaf physiological parameters obtained in November–December, 2011, the measurement closest to the simulated period.

The soil CO_2 efflux was measured manually at 1100–1600LT in 15 October 2011 using a diffusion-type CO_2 sensor (GMP343, Vaisala) connected to a PVC chamber (20 cm diameter, 15 cm height, and 1 cm soil depth-inserted) at 33 points in the study plot. Soil CO_2 efflux data were averaged over the plot as 3.18 ± 1.82 μmol m^{-2} s^{-1} (average soil respiration rate (R_{soil}) ± SD). Since there were small variations in soil temperature (average ± SD = 29.6 ± 0.6), the dependency of the R_{soil} on temperature could not be discerned. Moreover, R_{soil} measurements on the other days in January, March, and May 2012 using a portable IRGA (LI-6400) connected to a chamber (6400-09 soil CO_2 efflux chamber, Li-Cor) yielded 3.34 ± 0.87, 2.48 ± 0.86, and 3.38 ± 1.24 (average ± SD) μmol m^{-2} s^{-1}, respectively, and while acknowledging that R_{soil} is very likely affected by seasonal soil moisture changes, the available data did not show clear relationships between seasonal variations in R_{soil} and temperature or soil moisture. Thus, the whole day R_{soil} during the study period was regarded as a constant of 3.18 μmol m^{-2} s^{-1}.

3.4. Canopy structure measurements

The vertical profiles of leaf area index (LAI) were measured at 1-m intervals along two vertical observation lines by a plant canopy analyzer (LAI-2000, Li-Cor) using the tower. Then, the vertical profile of leaf area density (a_{leaf}) was calculated (Fig. 2a), and the LAI was determined to be 3.89 m^2 m^{-2} (in August, 2011), which is consistent with values estimated from observations of its spatial variation in the studied plot. The crown space was limited to the upper 3–4 m, beneath which the trunk space has few branches. Regular LAI observations through a whole year showed that the LAI reached up to 4–5 in summer (August–September), and that leaf abscission began in early-January and leaf-out occurred in the end of January.

The canopy clumping factor (Ω), which is a critical parameter for this study's model, was evaluated according to Chen and Cihlar (1995) concept with some modifications. Review and description of the observation and calculation are provided below.

The transmitted photosynthetic photon flux density (PPFD) through the canopy was measured at approximately 1-m above the forest floor along 53.6-m and 60.3-m straight transects by a quantum sensor (MIJ-14PAR, Environmental Measurement Japan Co. Ltd., Fukuoka, Japan) mounted at one end of supporting arm with a data logger (CR1000). In this study plot, the two transects were randomly determined in approximately northwest–southeast and northeast–southwest directions. The data logger sampled the PPFD at 0.03-s intervals. Thus, with a walking speed of 0.67 m s^{-1}, a PPFD output was sampled every 2-cm interval along each transect.

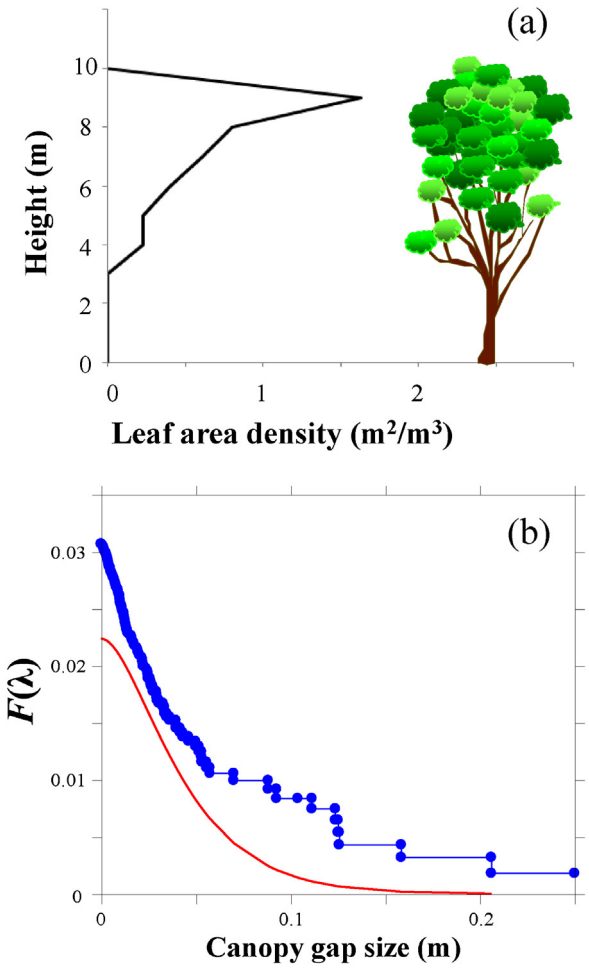

Fig. 2. (a) Vertical distribution of leaf area density, and (b) the fraction of the transects occupied by gaps larger than the indicated canopy gap size, λ, ($F(\lambda)$). Solid circles connected with a line indicate measured values of $F(\lambda)$ and theoretical $F(\lambda)$ for random gap is shown as a smooth curve.

In the distribution of the measured instantaneous PPFD, we can obtain a minimum (P_{min}) and a maximum (P_{max}) PPFD, which represent a steady baseline generated by the diffuse component and the direct component above the canopy, respectively. Note that P_{max} can be also obtained in the center of a large gap. Criteria for determining a sunfleck along the transect is (Chen and Cihlar, 1995): (i) any significant increase (>1%) in the PPFD value from the P_{min} or reversal of a decreasing trend indicates the beginning of sunfleck. (ii) The end of a sunfleck is determined when either the PPFD reaches the P_{min} or the beginning of a new sunfleck is detected. In reality, a canopy gap at some height results in a sunfleck on the forest floor with a width much larger than the gap because of the penumbra effect by the Sun. Based on the mass conservation principle, the total PPFD reaching the forest floor in the sunfleck should be equal to the total incident PPFD passing through the gap, represented as $\lambda P_{max} = \int_0^{\lambda_s} P(x)dx$ (where λ and λ_s are the canopy gap size and the apparent sunfleck width, respectively, and $P(x)$ is the measured PPFD at location x within the sunfleck). Using this equation and the direct PPFD measured at the forest floor along the

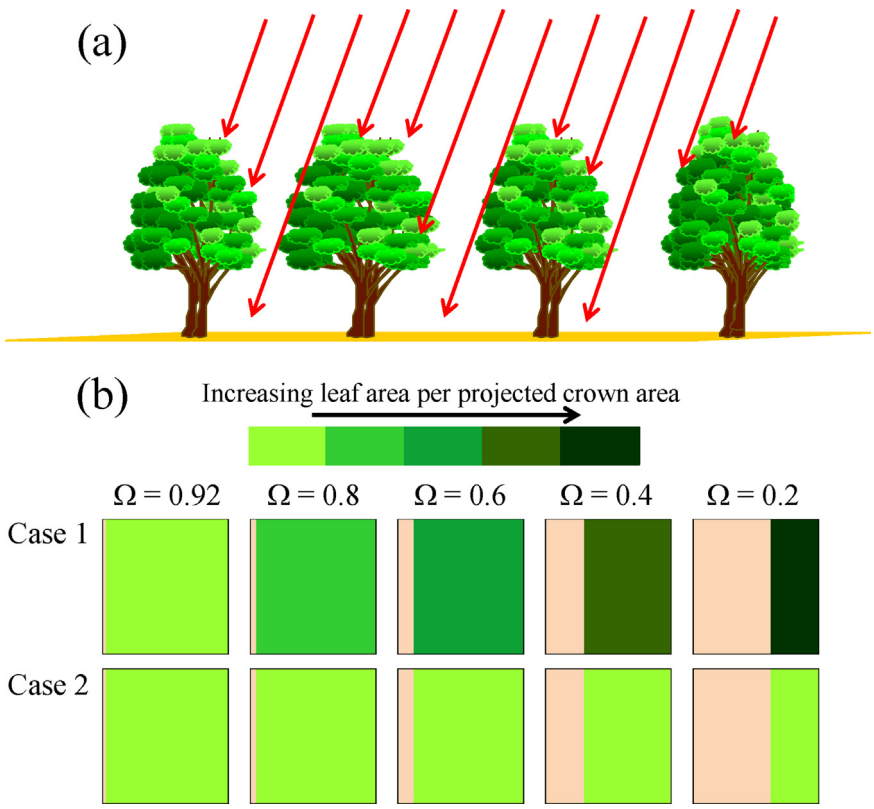

Fig. 3. (a) Radiation penetration through a rubber plantation canopy with regular gaps. (b) Schematic canopy gap fractions corresponding to different values of clumping factor (Ω). The green area in each box denotes the fraction of area occupied by leaves (AL), and the beige area represents the gap fraction. Case 1: leaf area index (LAI) is constant with changing values of Ω, and thus the leaf density of the AL increases with decreasing values of Ω, and Case 2: the leaf density of the AL remains the same, and thus LAI decreases with decreasing Ω.

transect, a probability distribution of λ, which is here represented as the fraction of the transects occupied by gaps larger than λ ($F(\lambda)$; Fig. 2b), can be obtained.

Following Chen and Black (1992), theoretical $F(\lambda)$ is given by

$$F(\lambda) = \left(1 + \frac{\mathrm{LAI_p}}{d_\mathrm{m}}\lambda\right) \exp\left[-\mathrm{LAI_p}\left(1 + \frac{\lambda}{d_\mathrm{m}}\right)\right] \quad (18)$$

where d_m is the characteristic dimension calculated as the square root of a leaf area, and $\mathrm{LAI_p}$ is the projected LAI onto a level surface calculated using the beam extinction coefficient (see Goudriaan, 1977). $\mathrm{LAI_p}$ for a perfect random canopy ($\mathrm{LAI_{pr}}$) can be calculated as $-\ln[F_\mathrm{m}(0)]$ (where $F_\mathrm{m}(0)$ is the measured $F(0)$), and thus, substituting this for Eq. (18) leads to the first estimate of random canopy-assumed $F_\mathrm{m}(\lambda)$ ($F_\mathrm{mr}{}^{(0)}(\lambda)$). Gaps appearing at probabilities in excess of $F_\mathrm{m}(\lambda)$ from $F_\mathrm{mr}{}^{(0)}(\lambda)$ are then removed or truncated, and after this first round of gap removal, $F_\mathrm{mr}{}^{(1)}(\lambda)$ is computed. In the next step, a new $\mathrm{LAI_{pr}}$ is assigned the value of $-\ln[F_\mathrm{mr}^{(1)}(0)]$, and substituting this for Eq. (18) produces a new $F_\mathrm{mr}{}^{(1)}(\lambda)$. $F_\mathrm{mr}{}^{(2)}(\lambda)$ can be estimated by gap-removing the new $F_\mathrm{mr}{}^{(1)}(\lambda)$ from the former $F_\mathrm{mr}{}^{(1)}(\lambda)$. In finding the final $F_\mathrm{mr}(\lambda)$, the removal of gaps appearing at probabilities in excess of $F_\mathrm{m}(\lambda)$ is repeated until $F_\mathrm{mr}{}^{(n+1)}(\lambda)$ is brought to the closest agreement with $F_\mathrm{mr}{}^{(n)}(\lambda)$.

Note that $F_\mathrm{m}(\lambda)$ and $F_\mathrm{mr}(\lambda)$ as the measured $F(\lambda)$ and the one assuming random canopy, respectively, for the studied plot are shown in Fig. 2b. Considering that removal or truncation of large gaps makes the canopy compacted, Chen and Cihlar (1995) derived from the beam extinction coefficient with taking into account the effect of the canopy clumping:

$$\Omega = \frac{[1 + F_\mathrm{m}(0) - F_\mathrm{mr}(0)]\ln[F_\mathrm{m}(0)]}{\ln[F_\mathrm{mr}(0)]} \quad (19)$$

Eq. (19) with $F_\mathrm{m}(0) = 0.031$ and $F_\mathrm{mr}(0) = 0.022$ (see Fig. 2b) yielded $\Omega = 0.92$ for the studied plot.

3.5. Simulations

We selected 10 simulation days, 5–14 August, 2011, from a wider study period. This period was selected because of the availability of the synchronous data of above-canopy CO_2 flux and the within-canopy storage flux (resulting in NEE estimates), above-canopy *LE*, leaf-level physiology, soil respiration, detailed description of canopy structure, and the occurrence of ideal environmental conditions, such as low rainfall (even though in the wet season), moist soil and day-to-day variations in radiation, temperature and humidity. In particular, because the main objective of this study was to develop a model that can describe the detailed canopy processes of rubber trees and to confirm its performance, reliable 30-min interval NEE data were required to compare the observation results and the model outputs.

The SVAT model in this study was parameterized by independently collected ecophysiological measurements and was not calibrated or parameterized by canopy-level flux measurements. Table 1 summarizes the major parameters used for model validation. After model validation using the canopy flux measurement, this model could be used to examine how the canopy/ecosystem fluxes were generated, and thus elucidate how the canopy structure (planting-spacing) controls the rubber plantation NEE and *LE*. For this purpose, we conducted two types of numerical experiments as follows.

The first numerical experiment was a model validation using all the measured canopy structure and ecophysiological parameters (see Table 1). Then, to examine the effect of the canopy clumping

Table 1
Major parameters used for model validation.[a]

Parameter	Value	Units
Latitude	11.95N	degrees
Longitude	105.57 E	degrees
Altitude	50	m
Canopy height	10	m
LAI	3.89	$m^2\ m^{-2}$
d_m	0.077	m
Ω	0.92	–
V_{cmax_25}	8.71 z − 30.6[b] (if V_{cmax_25} < 30, then V_{cmax_25} = 30)	$\mu mol\ m^{-2}\ s^{-1}$
J_{max}	2 V_{cmax}	$\mu mol\ m^{-2}\ s^{-1}$
R_d	0.02 V_{cmax}	$\mu mol\ m^{-2}\ s^{-1}$
m_L	8.9	–
b_L	0.03	$mol\ m^{-2}\ s^{-1}$
R_{soil}	3.18	$\mu mol\ m^{-2}\ s^{-1}$

[a] Symbols are represented in text.
[b] z denotes height (m) from the ground.

factor (Ω) on the canopy/ecosystem fluxes, we conducted two additional simulations in which Ω was varied while: total leaf area per ground area (LAI) was held constant at 3.89 (Case 1 in Fig. 3b), and total leaf area per crown area was held constant (Case 2 in Fig. 3b). Put differently, Cases 1 and 2 assume a change in foliage clumping with tree-to-tree spacing held constant and a change in tree-to-tree spacing with each individual tree's total leaf area held constant, respectively. It should be further instructive to note that in terms of agroforestry, Case 1 corresponds to larger inter-row spacing and denser intra-row leaf area, while Case 2 corresponds only to larger inter-row spacing or lower density of planted trees.

4. Results and discussion

4.1. Model validation

Availability of net ecosystem CO_2 exchange (NEE) data during the study period 5–14 August 2011 was 81.9% due to occasional failures of the within-canopy storage flux observation system. Here, we note that the diurnal variations in NEE differed from the observed above-canopy CO_2 flux because of within-canopy CO_2 storage. Above-canopy flux reached a maximum negative value higher than $-20\ \mu mol\ m^{-2}\ s^{-1}$ at around noon, while the peak within-canopy flux was around $-6\ \mu mol\ m^{-2}\ s^{-1}$ at 0700–0800LT (data not shown). Fig. 4 illustrates the measured diurnal patterns of NEE and *LE*, by combining all data during the study period and plotting only the data from the interquartile range, which reduces the influence of outliers. The extreme values of NEE and *LE* exceeded $-20\ \mu mol\ m^{-2}\ s^{-1}$ and around $600\ W\ m^{-2}$, respectively. Their daily accumulation calculated from the second quartile data were $2.24\ gC\ m^{-2}\ day^{-1}$ and $4.28\ mm\ day^{-1}$, respectively. Based on comparison with data reported on an annual basis (e.g., Malhi et al., 1999; Giambelluca et al., 2009; Costa et al., 2010), these results are consistent with reports speculating that rubber trees could be large carbon sinks and behave as 'water pumps' (see Mann, 2009; Qiu, 2009; Ziegler et al., 2009b, 2012; Tan et al., 2011).

All model computation results for the study period, i.e., including simulations against measurements out of the range between the first and third quartiles, are also plotted in Fig. 4. Overall, both the calculated NEE and *LE* capture the canonical form of the measured values, showing our SVAT model's ability to synthesize canopy transport of CO_2 and H_2O. Fig. 5 shows further comparisons of modeled NEE and *LE* and measurements. No significant differences between the modeled and the measured NEE (Fig. 5a) and *LE* (Fig. 5b) were observed (*t*-test, $P = 0.64$ and 0.50, respectively). The slopes and the intercepts of the regression lines for NEE and *LE* were both close to unity and zero, respectively, with strong

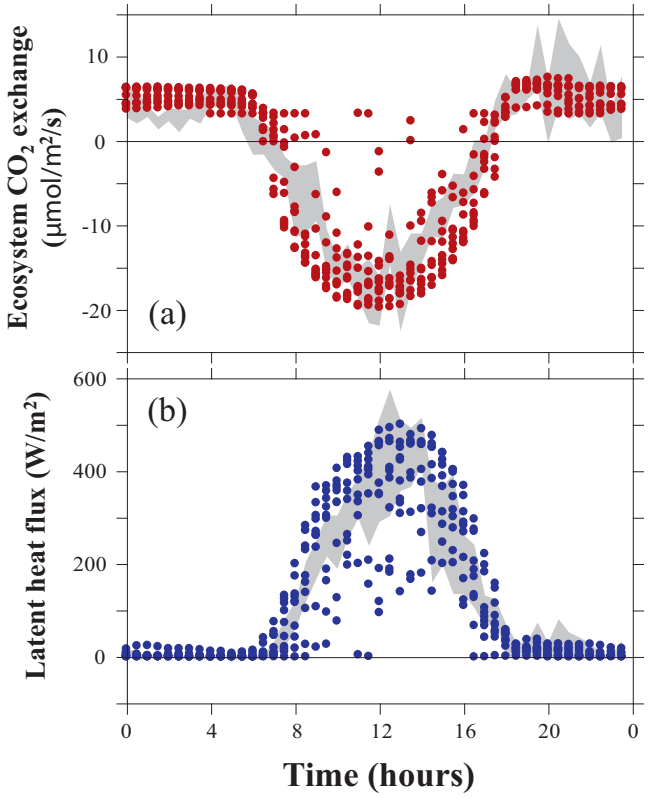

Fig. 4. Mean diurnal cycles of measured (gray zones) and modeled (solid circles) ecosystem CO_2 exchange (a) and latent heat flux (b) for 5–14 (10 days) August 2011. The gray zone denotes the range of the middle two quartiles of observations in the study period.

coefficients of determination (Fig. 5a: $y = 1.08x - 0.34$, $R^2 = 0.85$, and Fig. 5b: $y = 1.00x + 10.6$, $R^2 = 0.89$).

This successful reproduction of the measured canopy fluxes might be attributed to appropriate observations of canopy process such as canopy structure and leaf-scale ecophysiology. The measured Ω (0.92) indicated that the foliage in the studied canopy is nearly randomly distributed in space. On the other hand, a very clumped canopy ($\Omega < 0.2$) was observed at the adjacent plot (clone of PB330, planted in 2001 (10 years old in 2011)) containing large gaps between planting-rows, i.e., a 6-m interval in north–south direction, and such highly clumped rubber tree canopies are apparently common in the studied rubber plantation. Thus, it is informative to investigate the impact of different values of Ω on the canopy flux formation. It is important to note that except for immature trees, i.e., before about 6 years after planting, variation in Ω among stands is likely related more to clone type than age.

In terms of individual-leaf physiological traits measurements, V_{cmax_25} values for the studied rubber trees were observed to be around 30–70 $\mu mol\ m^{-2}\ s^{-1}$ at heights of 7–10 m. This range is consistent with prior reported values obtained for 2-year-old individuals of three different rubber tree clones (Kositsup et al., 2010). It is also comparable with values of upper canopy trees in Amazonian and Bornean tropical rain forests (e.g., Carswell et al., 2000; Kenzo et al., 2006), which in turn, were not significantly different from V_{cmax_25} reported for a large number of temperate broad-leaved tree species (see Wullschleger, 1993). Hence, the higher NEE and *LE* for the study site compared with trees in the temperate zone might be mainly attributed to higher incident radiative energy in the tropics, and the ecophysiological traits of rubber trees are secondary reason for it.

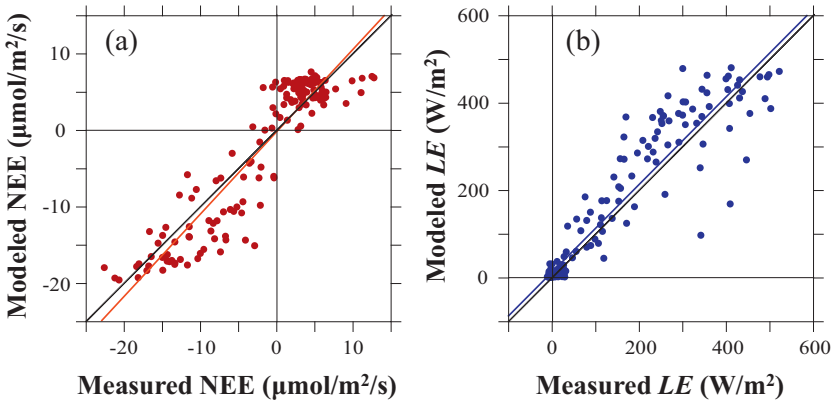

Fig. 5. Comparison between measured and modeled ecosystem CO_2 exchange (a: NEE) latent heat flux (b: *LE*). 1:1 and linear regression (a: $y = 1.08x - 0.34$, $R^2 = 0.85$, b: $y = 1.00x + 10.6$, $R^2 = 0.89$) lines are also shown.

4.2. Impact of clumping factor holding total leaf area per ground area constant (Case 1)

For both NEE and *LE* fluxes, a decrease in Ω from 1.0 to 0.8 had little effect on fluxes, while lowering Ω below 0.6 changed fluxes appreciably (Figs. 6a and 7a). Fluctuations in NEE and *LE* fluxes at the shorter timescale than the diurnal cycle became smaller and larger, respectively, with decreasing Ω. In particular, *LE* flux tended to be depressed in the morning and rise in the afternoon (Fig. 7a).

Figs. 6b and 7b show that decreases in source strengths at their peaks in accordance with decreases in Ω reduced NEE and *LE* fluxes. With decreasing Ω, source strengths in the upper canopy decreased, while those in the lower canopy slightly increased. This implies that the decrease in Ω enables light to penetrate deeper into the canopy, but in our study's case, the intensive source strengths in the upper canopy control the ecosystem fluxes because of concentrated foliage there (Figs. 6b and 7b).

Also, this implies that under conditions of moderate leaf amount and V_{cmax} in the lower canopy (see Kositsup et al., 2010) and relatively high quantum yield of the leaves, there is likely to be increases in ecosystem fluxes with decreasing Ω (see Baldocchi and Meyers, 1998). An optimum Ω for maximizing the fluxes is therefore likely to exist. Here we emphasize that the simulation results in this study were obtained using characteristics of physiology and canopy structure of the particular rubber tree under study, i.e., clone type and tree size/age.

4.3. Impact of clumping factor holding total leaf area per crown area constant (Case 2)

In the Case 2 simulations, the foliage amount of each individual tree can be assumed to be constant because total leaf area per projected crown area does not change (see Case 2 in Fig. 3b), and thus, variations in Ω can be assumed to correspond to those in tree-to-tree or inter-row spacing. Changing the planting spacing should likely change the LAI (i.e., leaf area per ground area).

Ground area-based fluxes of both NEE and *LE* decreased with decreasing LAI (Figs. 8a and 9a). In reality, soil respiration tends to decrease with decreasing LAI as an index of site productivity (Reichstein et al., 2003). Therefore, the extent to which the plantation became a CO_2 source at low LAI because of a large contribution by soil respiration (Fig. 8a) may be overestimated by the model because soil respiration was treated as a constant value. Changes in Ω in the range of 1.0–0.4 had little impact on CO_2 flux per leaf area (Fig. 8c). At $\Omega = 0.4$, the decrease in upper-canopy CO_2 source strength was compensated by an increase in lower-canopy source strength (Fig. 8d). The CO_2 flux per leaf area abruptly decreased at $\Omega = 0.2$ (Fig. 8c) owing to a drastic decrease in the light availability in the upper layer (Fig. 8d).

LE flux per leaf area decreased with decreasing Ω at around 1000–1300LT (Fig. 9c). However, decreasing Ω had little effect on daily *LE* because of enhanced *LE* fluxes in the afternoon. For both leaf area based fluxes of CO_2 and H_2O, source strengths in the

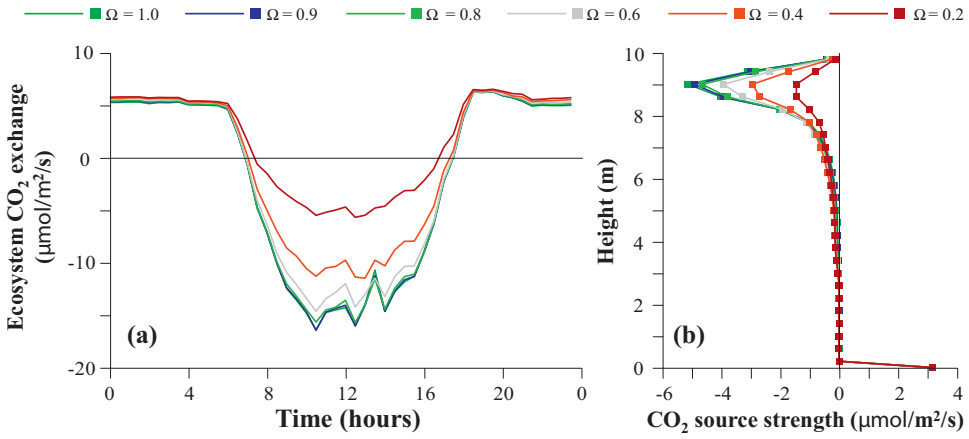

Fig. 6. Mean diurnal cycles of modeled ecosystem CO_2 exchange (a) and vertical profiles of the average modeled midday (1100–1300LT) CO_2 source strength as a function of canopy height (b), for canopy clumping factors (Ω) of 1.0, 0.9, 0.8, 0.6, 0.4 and 0.2, while total leaf area per ground area (LAI) of 3.89 is held constant (see Case 1 of Fig. 3b).

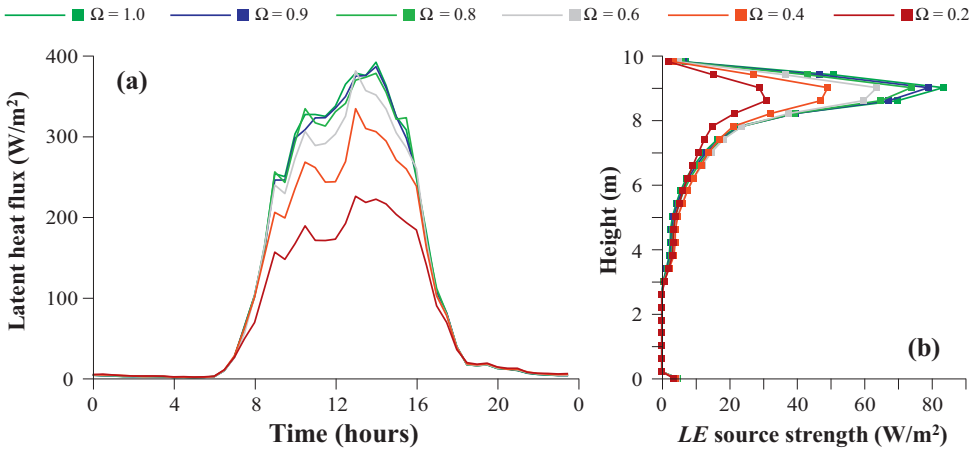

Fig. 7. Mean diurnal cycles of modeled ecosystem latent heat flux (*LE*) (a) and vertical profiles of the average modeled midday (1100–1300LT) *LE* source strength as a function of canopy height (b), for canopy clumping factors (Ω) of 1.0, 0.9, 0.8, 0.6, 0.4 and 0.2, while total leaf area per ground area (LAI) of 3.89 is held constant (see Case 1 of Fig. 3b).

upper canopy decreased with decreasing Ω, while source strengths in the lower canopy increased with decreasing Ω. The effects of decreasing Ω were more marked for Case 1 than for Case 2.

4.4. Optimal spacing for planting rubber trees

To determine the optimal value of Ω for maximizing primary productivity and water use efficiency, we delineated relationships between Ω and average net assimilation rate (A_n), latent heat flux (*LE*) and A_n/*LE* around midday (1100–1300LT) (Fig. 10). Ground area based A_n rates for both Cases 1 and 2 were least affected by Ω in the range of 1.0–0.8 (Figs. 10a-1 and b-1). Considering Fig. 8c, it could be expected that there was an optimum Ω for maximizing individual-level A_n in Case 2. Indeed, the A_n per leaf area peaked at $\Omega = 0.6$ (Fig. 10c-1).

The average *LE* around noon decreased with decreasing Ω (Fig. 10a-2, b-2, and c-2). This reduction was remarkable at around $\Omega = 0.6$. Finally, we found that ground area-based A_n/*LE* were maximized at $\Omega = 0.8$ for Case 1 (Fig. 10a-3) and $\Omega = 0.6$ for Case 2 (Fig. 10b-3), and that, unexpectedly, individual-level A_n/*LE* peaked at $\Omega = 0.4$ (Fig. 10c-3). However, since daily total leaf-scale *LE* was little affected by Ω variations, it is conceivable that the water use efficiency was maximized at $\Omega = 0.6$.

Thus we could conclude there was little difference in ground area-based productivity and water use efficiency between Ω at the range of 1.0–0.8 for either case, but individual-based productivity

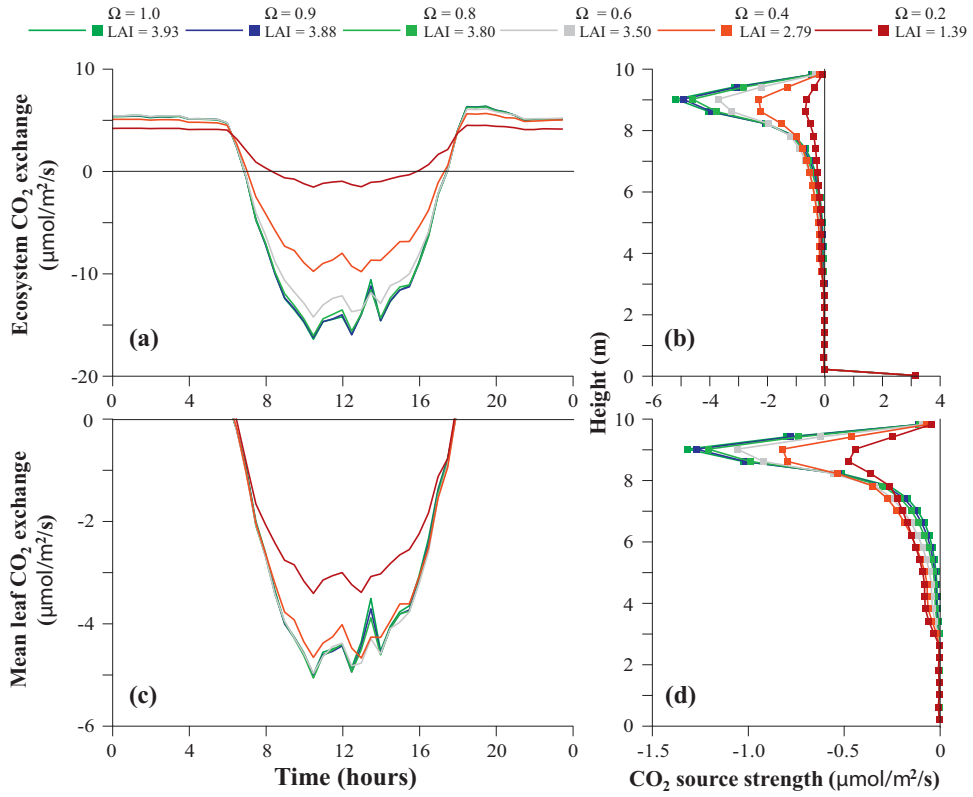

Fig. 8. Mean diurnal cycles of modeled ecosystem (a) and mean leaf (c) CO_2 exchange and mean vertical profiles of the average modeled midday (1100–1300LT) CO_2 source strength per ground area (b) and per leaf area (d) within each canopy layer as a function of canopy height, for canopy clumping factors (Ω) of 1.0, 0.9, 0.8, 0.6, 0.4 and 0.2, while total leaf area per crown area is held constant (see Case 2 of Fig. 3b).

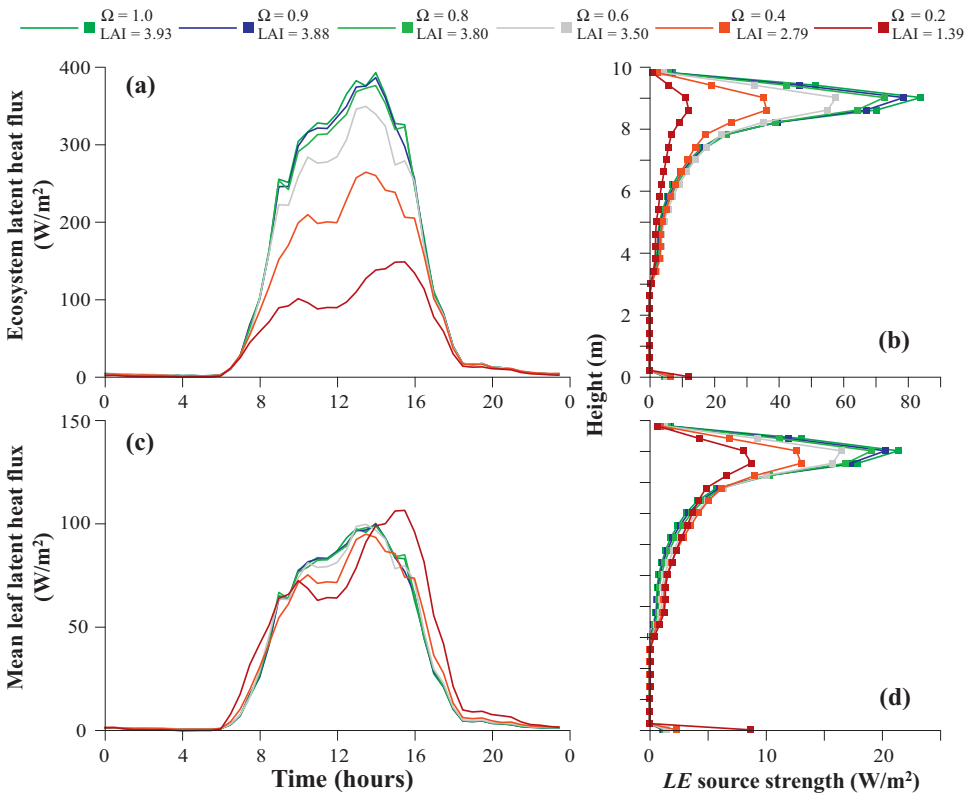

Fig. 9. Mean diurnal cycles of modeled ecosystem (a) and mean leaf (c) latent heat flux (*LE*) and mean vertical profiles of the average modeled midday (1100–1300LT) *LE* source strength per ground area (b) and per leaf area (d) within each canopy layer around noon as a function of canopy height, for canopy clumping factors (Ω) of 1.0, 0.9, 0.8, 0.6, 0.4 and 0.2, while total leaf area per crown area is held constant (see Case 2 of Fig. 3b).

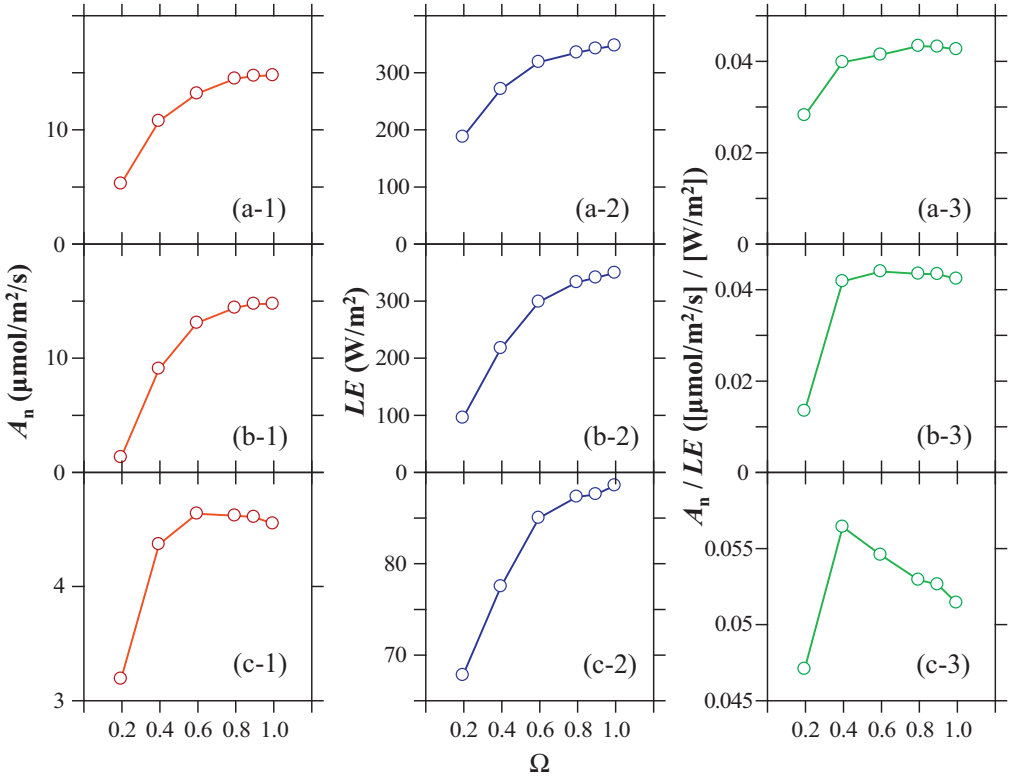

Fig. 10. Relationships between the canopy clumping factor (Ω) and average midday (1100–1300LT) net assimilation rate (A_n) (a, b, and c-1), latent heat flux (*LE*) (a, b, and c-2) and water use efficiency (A_n/*LE*) (a, b, and c-3). Ω varies while total leaf area per ground area (LAI) of 3.89 is held constant (see Case 1 of Fig. 3b) (a-1, 2, and 3) and while total leaf area per crown area is held constant (see Case 2 of Fig. 3b) (b-1, 2, and 3) and (c-1, 2, and 3). Values in (a-1, 2, and 3) and (b-1, 2, and 3) are per ground area, and in (c-1, 2, and 3) are per leaf area.

and water use efficiency were maximized at $\Omega = 0.6$. This Ω value (0.6) can be roughly estimated to be the regular spacing at 6.8 m in one direction with 3-m in its normal direction. The regular spacing of 6-m and 3-m in Cambodia and 7-m and 3-m in Thailand (e.g., Kositsup et al., 2010) are commonly used because they provide management convenience and a relatively high density of trees. However, it is interesting to note that those common planting-spacings are consistent with the spacing estimated as optimal for maximizing rubber tree primary productivity.

5. Conclusions

Using a combination of elaborate eddy covariance observations for NEE and *LE*, detailed leaf-level physiology measurements (including their vertical profiles within the canopy), measurements of canopy structure peculiar to rubber plantations, and a multilayer SVAT model applicable to the rubber plantations, we examined how the peculiar canopy structure, i.e., the foliage clumping factor (Ω) generated by planting trees with regular spacing, affects the NEE and *LE* of the studied rubber plantation. Furthermore, we revisited the meanings of Ω and its evaluation. We also examined the planting-spacing optimum for maximizing rubber plantation primary productivity by numerical experiments with the validated SVAT model. Although the results of the numerical experiments are site-specific with respect to clone and stand age, the methods allowed us to consider the effects of intensive foliage clumping on forest canopy fluxes in general. Results of the numerical experiments showed that the SVAT model performed well and can be used as a tool to investigate the impact of land use change, e.g., from pre-existing vegetation to rubber plantation, on local water and carbon cycling.

Acknowledgements

This study was initiated as cooperative project between Cambodian Rubber Plantation Department, Cambodian Rubber Research Institute (CRRI), University of Hawai'i, and Kyushu University, supported by the Global COE (Centers of Excellence) Program (GCOE) of the Japan Society for the Promotion of Science (JSPS) and a grant from Kyushu University. We acknowledge help given by the staff of CRRI and other contributors, including Hiroki Tanaka, Tsuyoshi Kajisa, Khun Kakada, Nobuya Mizoue, Makiko Tateishi, and Tetsukazu Yahara.

This study was conducted primarily under the project "Estimation and simulation of carbon stock change of tropical forest in Asia (2011–2014)" funded by the Ministry of Agriculture, Forestry and Fisheries, Japan. Also, this study was supported by in part by a Grant-in-Aid for Scientific Research (# 23405028) and the granted project "Program for risk information on climate change" from the Ministry of Education, Science and Culture, Japan. Participation of RGM, WL, TWG, MH, and QS was supported by NASA grants NNG04GH59G and NNX08AL90G. MH was supported by the US Department of Energy (DOE) Biological and Environmental Research (BER) Earth System Modeling (ESM) program. Pacific Northwest National Laboratory (PNNL) is operated for the US DOE by Battelle Memorial Institute under Contract DE-AC05-76RL01830. ADZ was supported by National University of Singapore (NUS) grant R-109-000-092-133 and Asia-Pacific Network for Global Change Research (APN) grant #ARCP2008-01CMY.

References

Association of Natural Rubber Producing Countries (ANRPC). Natural Rubber Trends & Statistics Archive. May 2010. http://www.anrpc.org/html/archive.aspx (last accessed 29.01.2012).

Badger, M.R., Collatz, G.J., 1977. Studies on the kinetic mechanism of ribulose-1,5-bisphosphate carboxlase and oxygenase reactions, with particular reference to the effect of temperature on kinetic parameters. Carnegie Institute of Washington Yearbook 76, 355–361.

Baldocchi, D., Meyers, T., 1998. On using eco-physiological, micrometeorological and biogeochemical theory to evaluate carbon dioxide, water vapor and trace gas fluxes over vegetation: a perspective. Agricultural and Forest Meteorology 90, 1–25.

Ball, J.T., Woodrow, I.E., Berry, J.A., 1987. A model predicting stomatal conductance and its contribution to the control of photosynthesis under different environmental conditions. In: Biggens, J. (Ed.), Progress in Photosynthesis Research. Mirtinus Nijhoff Publishers, The Netherlands, pp. 221–224.

Campbell, G.S., Norman, J.M., 1998. An Introduction to Environmental Biophysics. Springer-Verlag, New York.

Carr, M.K.V., 2012. The water relations of rubber (*Hevea brasiliensis*): a review. Experimental Agriculture 48, 176–193.

Carswell, F.E., Meir, P., Wandelli, E.V., Bonates, L.C.M., Kruijt, B., Barbosa, E.M., et al., 2000. Photosynthetic capacity in a central Amazonian rain forest. Tree Physiology 20, 179–186.

Chen, J.M., Black, T.A., 1992. Foliage area and architecture of plant canopies from sunfleck size distributions. Agricultural and Forest Meteorology 60, 249–266.

Chen, J.M., Cihlar, J., 1995. Plant canopy gap-size analysis theory for improving optical measurements of leaf-area index. Applied Optics 34, 6211–6222.

Chen, Q., Baldocchi, D., Gong, P., Dawson, T., 2008. Modeling radiation and photosynthesis of a heterogeneous savanna woodland landscape with a hierarchy of model complexities. Agricultural and Forest Meteorology 148, 1005–1020.

Collatz, G.J., Ball, J.T., Grivet, C., Berry, J.A., 1991. Regulation of stomatal conductance and transpiration: a physiological model of canopy processes. Agricultural and Forest Meteorology 54, 107–136.

Costa, M.H., Biajoli, M.C., Sanches, L., Malhado, A.C.M., Hutyra, L.R., da Rocha, H.R., et al., 2010. Atmospheric versus vegetation controls of Amazonian tropical rain forest evapotranspiration: are the wet and seasonally dry rain forests any different? Journal of Geophysical Research 115, G04021, http://dx.doi.org/10.1029/2009JG001179.

de Pury, D.G.G., Farquhar, G.D., 1997. Simple scaling of photosynthesis from leaves to canopies without the errors of big-leaf models. Plant, Cell & Environment 20, 537–557.

Farquhar, G.D., Wong, S.C., 1984. An empirical model of stomatal conductance. Australian Journal of Plant Physiology 11, 191–210.

Farquhar, G.D., von Caemmerer, S., Berry, J.A., 1980. A biochemical model of photosynthetic CO_2 assimilation in leaves of C3 species. Planta 149, 78–90.

Fox, J., Vogler, J.B., Sen, O.L., Giambelluca, T.W., Ziegler, A.D., 2012. Simulating land-cover change in montane mainland Southeast Asia. Environmental Management 49, 968–979.

Giambelluca, T.W., Martin, R.E., Asner, G.P., Huang, M., Mudd, R.G., Nullet, M.A., DeLay, J.K., Foote, D., 2009. Evapotranspiration and energy balance of native wet montane cloud forest in Hawai'i. Agricultural and Forest Meteorology 149, 230–243.

Goudriaan, J., 1977. Crop Micrometeorology: A Simulation Study. Center for Agricultural Publishing and Documentation, Wageningen.

Guardiola-Claramonte, M., Troch, P.A., Ziegler, A.D., Giambelluca, T.W., Durcik, M., Vogler, J.B., et al., 2010. Hydrologic effects of the expansion of rubber (*Hevea brasiliensis*) in a tropical catchment. Ecohydrology 3, 306–314.

Isarangkool Na Ayutthaya, S., Do, F.C., Pannangpetch, K., Junjittakarn, J., Maeght, J.-L., Rocheteau, A., Cochard, H., 2011. Water loss regulation in mature *Hevea brasiliensis*: effects of intermittent drought in the rainy season and hydraulic regulation. Tree Physiology 31, 751–762.

Kenzo, T., Ichie, T., Watanabe, Y., Yoneda, R., Ninomiya, I., Koike, T., 2006. Changes in photosynthesis and leaf characteristics with tree height in five dipterocarp species in a tropical rain forest. Tree Physiology 26, 865–873.

Kormann, R., Meixner, F.X., 2001. An analytical footprint model for non-neutral stratification. Boundary-Layer Meteorology 99, 207–224.

Kositsup, B., Kasemsap, P., Thanisawanyangkura, S., Chairungsee, N., Satakhun, D., Teerawatanasuk, K., et al., 2010. Effects of leaf age and position on light-saturated CO_2 assimilation rate, photosynthetic capacity, and stomatal conductance in rubber trees. Photosynthetica 48, 67–78.

Kumagai, T., Kume, T., 2012. Influences of diurnal rainfall cycle on CO_2 exchange over Bornean tropical rainforests. Ecological Modelling 246, 91–98.

Kumagai, T., Ichie, T., Yoshimura, M., Yamashita, M., Kenzo, T., Saitoh, T.M., et al., 2006. Modeling CO_2 exchange over a Bornean tropical rain forest using measured vertical and horizontal variations in leaf-level physiological parameters and leaf area densities. Journal of Geophysical Research 111, http://dx.doi.org/10.1029/2005JD006676.

Malhi, Y., Baldocchi, D.D., Jarvis, P.G., 1999. The carbon balance of tropical, temperate and boreal forests. Plant, Cell & Environment 22, 715–740.

Mann, C.C., 2009. Addicted to rubber. Science 325, 564–566.

Manzoni, S., Katul, G., Fay, P.A., Polley, H.W., Porporato, A., 2011. Modeling the vegetation-atmosphere carbon dioxide and water vapor interactions along a controlled CO_2 gradient. Ecological Modelling 222, 653–665.

Priyadarshan, P.M., 2003. Breeding *Hevea brasiliensis* for environmental constraints. Advances in Agronomy 79, 351–400.

Priyadarshan, P.M., Hoa, T.T.T., Huasun, H., Goncalves PdS., 2005. Yielding potential of rubber (*Hevea brasiliensis*) in sub-optimal environments. In: Kang, M.S. (Ed.), Genetic and Production Innovations in Field Crop Technology: New Development in Theory and Practice. The Haworth Press, Inc., Philadelphia, pp. 221–247.

Qiu, J., 2009. Where the rubber meets the garden. Nature 457, 246–247.

Reichstein, M., Rey, A., Freibauer, A., Tenhunen, J., Valentini, R., Banza, J., et al., 2003. Modeling temporal and large-scale spatial variability of soil respiration from

soil water availability, temperature and vegetation productivity indices. Global Biogeochemical Cycles 17, 1104, http://dx.doi.org/10.1029/2003GB002035.
Simien, A., Penot, E., 2011. Current evolution of smallholder rubber-based farming systems in southern Thailand. Journal of Sustainable Future 30, 247–260.
Tan, Z-H., Zhang, Y-P., Song, Q-H., Liu, W-J., Deng, X-B., Tang, J-W., et al., 2011. Rubber plantations act as water pumps in tropical China. Geophysical Research Letters 38, L24406, http://dx.doi.org/10.1029/2011GL050006.
Tanaka, K., Takizawa, H., Tanaka, N., Kosaka, I., Yoshifuji, N., Tantasirin, C., et al., 2003. Transpiration peak over a hill evergreen forest in northern Thailand in the late dry season: assessing the seasonal changes in evapotranspiration using a multilayer model. Journal of Geophysical Research D17, 4533, http://dx.doi.org/10.1029/2002JD003028.
Tanaka, K., Takizawa, H., Kume, T., Xu, J., Tantasirin, C., Suzuki, M., 2004. Impact of rooting depth and soil hydraulic properties on the transpiration peak of an evergreen forest in northern Thailand in the late dry season. Journal of Geophysical Research 109, D23107, http://dx.doi.org/10.1029/2004JD004865.
von Caemmerer, S., Farquhar, G.D., 1981. Some relationships between the biochemistry of photosynthesis and the gas exchange of leaves. Planta 153, 376–387.
von Caemmerer, S., Evans, J.R., Hudson, G.S., Andrews, T.J., 1994. The kinetics of ribrose-1, 5-bisphosphate carboxylase/oxygenase in vivo inferred from measurements of photosynthesis in leaves of transgenic tabaco. Planta 195, 88–97.
Watanabe, T., Mizutani, K., 1996. Model study on micrometeorological aspects of rainfall interception over an evergreen broadleaved forest. Agricultural and Forest Meteorology 80, 195–214.
Wauters, J.B., Coudert, S., Grallien, E., Jonard, M., Ponette, Q., 2008. Carbon stock in rubber tree plantations in Western Ghana and Mato Grosso (Brazil). Forest Ecology and Management 255, 2347–2361.
Wu, Z-L., Liu, H-M., Liu, L-Y., 2001. Rubber cultivation and sustainable development in Xishuangbanna, China. International Journal of Sustainable Development & World Ecology 8, 337–345.
Wullschleger, S.D., 1993. Biochemical limitations to carbon assimilation in C3 plants – a retrospective analysis of the A/Ci curves from 109 species. Journal of Experimental Botany 44, 907–920.
Ziegler, A.D., Bruun, T.B., Guardiola-Claramonte, M., Giambelluca, T.W., Lawrence, D., Nguyen, T.L., 2009a. Environmental consequences of the demise in swidden agriculture in SE Asia: hydrology and geomorphology. Human Ecology 37, 361–373.
Ziegler, A.D., Fox, J.M., Xu, J., 2009b. The rubber juggernaut. Science 324, 1024–1025.
Ziegler, A.D., Phelps, J., Yuen, J.Q., Webb, E.L., Lawrence, D., Fox, J.M., et al., 2012. Carbon outcomes of major land-cover transitions in SE Asia: great uncertainties and REDD+ policy implications. Global Change Biology 18, 3087–3099.